




Article

Novel Modeling for the Calculation of the Center of Lateral Resistance Position of Different Ships Making Use of a Full Mission Bridge Simulator and AI Tools

José M. Pérez-Canosa , Francisco Javier Lama-Carballo, Alsira Salgado-Don, Genaro Cao-Feijóo ,
Eliseo A. Pacheco and José A. Orosa * 

Department of Navigation Sciences and Marine Engineering, University of A Coruña, Paseo de Ronda, 51, 15011 A Coruña, Spain; jose.pcanosa@udc.es (J.M.P.-C.); javier.lama@udc.es (F.J.L.-C.); alsira.salgado@udc.es (A.S.-D.); genaro.cao@udc.es (G.C.-F.); eliseo.pacheco@udc.es (E.A.P.)

* Correspondence: jose.antonio.rosa@udc.es; Tel.: +34-981-167-000 (ext. 4320)

Abstract: Ship maneuvering in ports is increasingly reduced because the increase in ship size is not proportional to the increase in port areas. Furthermore, the number of assisted vessels and the need for tugboats working in densely populated areas make it necessary to reduce the number of involved tugboats, reducing pollution and costs. Therefore, shiphandlers must know, in addition to the pivot point, the center of lateral resistance under any circumstance to optimize the assistance from tugboats and improve maritime navigation. From the literature, it is evident that the practical determination of the center of lateral resistance is still unknown. This paper aims to propose novel mathematical models to identify the position of this point and the most important variables that determine its position. For that, data of different ships in different conditions were obtained from a full mission bridge simulator. Afterwards, 15 novel mathematical models were developed, making use of artificial intelligence tools and training neural networks. The high determination factor reached in some models shows the accuracy of the obtained models. One advantage of the presented models is that they are very easy to be applied by shiphandlers, because highly well-known parameters are involved. Moreover, original 3D charts showing the combination of the input variables were generated to identify the map of the whole process. The very simple new models obtained and the novel 3D charts shown in the present paper can be considered useful and applicable by the shiphandlers of most of the merchant fleet to improve the efficiency and safety of maritime navigation in increasingly restricted waters.

Keywords: full bridge and navigation simulator; center of lateral resistance; rate of turn; mathematical models; artificial intelligence



Citation: Pérez-Canosa, J.M.; Lama-Carballo, F.J.; Salgado-Don, A.; Cao-Feijóo, G.; Pacheco, E.A.; Orosa, J.A. Novel Modeling for the Calculation of the Center of Lateral Resistance Position of Different Ships Making Use of a Full Mission Bridge Simulator and AI Tools. *J. Mar. Sci. Eng.* **2024**, *12*, 1381. <https://doi.org/10.3390/jmse12081381>

Academic Editor: Anatoly Gusev

Received: 3 July 2024

Revised: 8 August 2024

Accepted: 12 August 2024

Published: 13 August 2024



Copyright: © 2024 by the authors. Licensee MDPI, Basel, Switzerland. This article is an open access article distributed under the terms and conditions of the Creative Commons Attribution (CC BY) license (<https://creativecommons.org/licenses/by/4.0/>).

1. Introduction

The use of simulators for testing and assessing the human operator's ability and performance is widely extended in maritime education and training [1,2], even for the tasks of supervising the navigation and the maneuverability of autonomous ships [3]. Furthermore, bridge simulators are not only used to assess human abilities, but they are also employed to propose novel models capable of providing solutions for predicting emissions from ships and tugboats during ship assistance [4]. Additionally, navigation simulators are being used to improve the safety of navigation during maneuvers in restricted areas with the use of an augmented virtual navigation information display [5]. As a result, the International Maritime Organization (IMO) has supported the use of simulators in maritime education as a training and teaching method, which improves the overall safety of navigation. The correct use of marine simulators is also included and regulated in the International Convention on Standards of Training, Certification, and Watchkeeping for Seafarers (STCW) [2]. Therefore, a certified simulator, as used in the present research,

can indicate the possible real effects of adequate conditions or actions in the navigation bridge [1] and, in consequence, the results obtained from it can be considered realistic enough of actual situations [6].

The number and size of the actual ships have increased in recent years, so the margin of safety of their maneuvers in restricted waters has been reduced [7]. For this reason, the presence of tugboats capable of providing the necessary assistance has become essential, although their operations are carried out in increasingly smaller areas. Furthermore, as these maritime assistances from tugboats to ships are performed near densely populated areas, there is a tendency to reduce the number of involved tugboats to minimize their emissions and to reduce costs for shipowners. However, it is often observed that in many ports and certain maneuvers, several tugboats remain on standby alongside the assisted vessel most of the time. These tugboats only act sporadically by pulling or pushing the ship in parallel approaching the berth. If the exact points at which to apply tugboat forces were known, employing fewer tugboats would suffice.

The accurate prediction of ship maneuvering characteristics is essential in preliminary design [8]. Additionally, a thorough knowledge of a ship's maneuverability from a handling perspective is crucial for shiphandlers (masters, officers, and pilots) to ensure navigation safety in restricted waters. Furthermore, adequate understanding of a ship's maneuverability by the shiphandlers allows for reducing external assistance (tugboats), thereby cutting economic costs and emissions.

As in other research carried out previously [8], in the present paper, the prediction of ship maneuverability is conducted using mathematical models, artificial intelligence (AI) and data obtained from tests in a navigation simulator. In the field of maneuverability, it is essential to know the position of the points around which the vessel moves, such as the pivot point (PP) and the center of lateral resistance (CLR).

The PP, described by some authors as an "apparent pivot point", is widely and traditionally used by many shiphandlers as an important point (crucial reference instead of "important point") to visualize the ship's rotation during combined rotation and translation movements [9]. The PP is defined as the point along the fore–aft axis of a turning ship that has no sideways movement, having for reference the surface of the water (the drift angle is zero) [10,11]. However, it is peripatetic, i.e., a non-stationary point, whose position continuously changes during the ship's displacement, depending on the numerous and variable involved forces as the inertia of rotation of the ship and the efficient lateral forces applied. Nevertheless, some studies argue that the understanding of the traditional concept of PP for maneuvering purposes and the shiphandler's knowledge may be flawed [10]. Therefore, in many situations, knowing the position of the CLR is more critical for shiphandlers than that of the PP.

The CLR (or neutral point) is defined as a physical point whose position depends on the ship's center of gravity, the center of buoyancy, the underwater area's center (hull shape and trim), and the pressure fields around the hull [9]. Additionally, it is considered as the point of the ship's centerline (fore–aft axis) where an effective lateral force causes no rotation [10]. On one hand, if the lateral force is only applied in the CLR position and has no arm lever, the ship then only experiences a sideways motion (no turning moment). On the other hand, if the transverse force is applied ahead of the CLR position, the ship experiences a non null rotation (rate of turn, ROT) to the port or starboard side. Therefore, the CLR and the PP are distinct centers, and applying a force (like from a tugboat) near the CLR produces less rotation and more translation).

Regarding the PP, for a long time, significant research on its influence on maneuverability has been published over the years. One of the recent studies was conducted by Serhii et al. [11], where they stated that all approaches to determining the PP position were not entirely accurate. In this research, the position of the PP relative to the center of rotation, instead of the center of gravity, was calculated. In the proposed linear mathematical model, the dependence of the rotation center motion on the longitudinal speed is shown.

Regarding the CLR, as previously mentioned, there is little information available about its study. In some studies, the researchers [10] consider that at the range of port operation speeds, the CLR position is close to midship, and if the ship has a trim by forward, this point is shifted a little more forward. If the ship is trimmed forward, this point shifts a little more forward, and if the ship is trimmed aft, it shifts a little more aft. These differences in movements toward forward and aft heads are considered less than 10% of the ship's length. Moreover, it is assumed that the CLR motion due to the speed is rarely more than 10% of the ship's length in the direction of the ship's movement. Therefore, there are no specific studies on the position of CLR point, taking into account all the traditional variables involved in ship maneuverability, which is essential to ensure the safety of navigation and reduce the required tugboats during assistance.

In the present paper, the CLR position of different types of ships sailing at different speeds is obtained after applying a transversal virtual force in the full mission bridge simulator. Afterwards, following the same approach as other research studies aimed at improving safety during sea navigation [12], artificial intelligence (AI) tools were used to obtain 15 novel mathematical models, some of which demonstrate a very high accuracy. Moreover, simple and useful equations relating the most significant variables are obtained, making them easily applicable for shiphandlers.

The remainder of the present paper is structured as follows: Section 2 presents the full mission bridge simulator used to obtain the CLR and describes the mathematical models employed by the mentioned simulator. The last sub-section shows the data collection of different ships (ships' particulars), and describes the methodological procedure followed when a large number of simulations were carried out. Section 3 shows the different and novel mathematical models proposed which were obtained using AI tools, comparing the precision between them. Furthermore, new 3D charts representing the variables of most influence are included. Section 4 discusses the obtained results, including some comments about the real accidents and the benefits of knowing the CLR position if a tugboat were available. Section 5 concludes the paper.

2. Materials and Methods

2.1. Transas 5000 Simulator Description

The School of Nautical and Marine Engineering (E.T.S Náutica y Máquinas) of the University of A Coruña (UDC) has, among others, the "Navi-Trainer Professional 5000", a full mission bridge and navigation simulator to be used by the deck students as future officers and masters. It was manufactured by the Norwegian company Transas. It enables the training and certification of watch officers, chief officers, masters and pilots serving on commercial and fishing ships with a gross tonnage of 500 tons and more in compliance with the requirements of IMO STCW 78/95 during training sessions on specialized courses. Furthermore, the simulator is capable of re-constructing and analyzing complex navigational situations, including emergencies in the actual seamanship.

The NTPRO 5000 simulator, shown in Figure 1, is a hard and software system consisting of dedicated and hands-on equipment of full mission navigation bridges operating under the instructor station control deployed on the basis of standard personal computers connected to a local computer network.

The software includes the program modules such as network operation manager; module for calculating mathematical models of ownships, target vessels, drifting objects, tugboats, model of 3D wind-induced waves, mooring lines, and fenders; the instructor's main display; a conning display; visual channels; and an interface with a real ship's equipment.

The simulator uses ready-to-use databases, which are permanently extended and updated: the library of visual 3D scenes of specific gaming areas, the library of radar scenes of the same areas, and the library of vessels' mathematical models.

Among others, this simulator has Statement of Compliance with Class A Standard for Certification of Maritime Simulators No. 2.14, October 2007, based on requirements of the STCW Convention, Regulation I/12, issued by DNV [8,9].



Figure 1. Vision of the full mission simulator with the steering instruments and some bridge equipment.

According to the specific needs and requirements, the software database allows the instructor to customize different scenarios considering different models of ships, navigational areas, weather and hydrological conditions, at any time of the day, reaching a final aspect from a visual and acoustic point of view highly realistic. The correctly adjusted mathematical ship models ensure the required realism of their behavior during navigation, mooring, towing, and other port operations in any adverse conditions.

2.2. Description of the Mathematical Models

The set of mathematical models for a maneuver simulator consists of mathematical models of ships, hardware models and environment element models. The motion of all the objects is modeled, including the mechanic and hydrodynamic interaction between objects and the environment (if necessary).

The ship motion mathematical model is based on a set of nonlinear differential equations. The set of equations' solutions was used to define the ship motion kinematics parameters, i.e., the ship center of gravity coordinates (x_g, y_g, z_g) , the inclination angles (roll, trim, and course), and the corresponding values of velocity and acceleration. Two coordinate systems are used: the fixed axes $(X_g O_g Z_g)$ —a right-hand orthogonal system nominally fixed to the Earth—and the body axes (XOZ) —a right-hand orthogonal system nominally fixed to the ship.

The fixed axes' origin lies in the fixed point O_g . The $O_g X_g$ axis and $O_g Y_g$ axis lie in the plane parallel to the calm free water surface, while the $O_g Z_g$ axis is perpendicular to the plane. The direction of the $O_g X_g$ axis is poleward, $O_g Y_g$ axis directs eastward and the $O_g Z_g$ axis directs downwards.

The body axes' origin is in the ship center of gravity. The OX axis and OY axis are parallel to the base plane, while the OZ axis is perpendicular to it. The direction of the OX axis is forward, OY axis toward starboard, and OZ downwards. Therefore, the equations describing the ship motion, expressed as force components, are as follows:

$$(m_A + \lambda_{11}) \cdot \frac{dV_X}{dt} + (m_A + \lambda_{22}) \cdot V_Y \omega_Z + (m_A + \lambda_{33}) \cdot V_Z \omega_Y = \sum F_X + \sum F_{X(M)}, \quad (1)$$

$$(m_A + \lambda_{22}) \cdot \frac{dV_Y}{dt} + (m_A + \lambda_{11}) \cdot V_Z \omega_X - (m_A + \lambda_{33}) \cdot V_Y \omega_X = \sum F_Y + \sum F_{Y(M)}, \quad (2)$$

$$(m_A + \lambda_{33}) \cdot \frac{dV_Z}{dt} - (m_A + \lambda_{11}) \cdot V_Z \omega_Y - (m_A + \lambda_{22}) \cdot V_Y \omega_Z = \sum F_Z + \sum F_{Z(M)}, \quad (3)$$

where m_A is the ship mass, calculated as follows:

$$m_A = \rho \cdot L \cdot B \cdot Dr \cdot BC, \tag{4}$$

where ρ is the water density; L is the ship's length; B is the ship's beam; Dr is the ship's draught at midship; and BC is the block coefficient, (see Appendix A).

$\sum F_X, \sum F_Y, \sum F_Z$ correspond to the total force components due to water and wind influence in the three axes.

$\sum F_{X(M)}, \sum F_{Y(M)}, \sum F_{Z(M)}$ represent the total mechanical force in the three axes.

$\lambda_{11}, \lambda_{22}, \dots, \lambda_{66}$ are the added masses.

$\lambda_{11}, \lambda_{22}, \dots, \lambda_{66}$ define the ship velocity components in the body axis.

V_X, V_Y, V_Z represent the ship angular velocity components in the body axis, which can be calculated as follows:

$$\omega_X = \theta - \varphi \cdot \sin \varphi, \tag{5}$$

$$\omega_Y = \psi \cdot \cos \theta + \varphi \cdot \cos \psi \cdot \sin \theta, \tag{6}$$

$$\omega_Z = \varphi \cdot \cos \psi \cdot \cos \theta - \psi \cdot \sin \theta, \tag{7}$$

where θ is the roll angle; φ is the course angle; and ψ is the pitch angle.

The corresponding total mechanical moment components can be expressed as follows:

$$(J_X + \lambda_{44}) \frac{d\omega_X}{dt} + [(J_Z + \lambda_{66}) - (J_Y + \lambda_{55})] \omega_Y \cdot \omega_Z + (\lambda_{33} - \lambda_{22}) V_Y \cdot V_Z = \sum M_X + \sum M_{X(M)}, \tag{8}$$

$$(J_Y + \lambda_{55}) \frac{d\omega_Y}{dt} + [(J_X + \lambda_{44}) - (J_Z + \lambda_{66})] \omega_X \cdot \omega_Z + (\lambda_{11} - \lambda_{33}) V_X \cdot V_Z = \sum M_Y + \sum M_{Y(M)}, \tag{9}$$

$$(J_Z + \lambda_{66}) \frac{d\omega_Z}{dt} + [(J_Y + \lambda_{55}) - (J_X + \lambda_{44})] \omega_X \cdot \omega_Y + (\lambda_{22} - \lambda_{11}) V_Y \cdot V_Z = \sum M_Z + \sum M_{Z(M)}, \tag{10}$$

where $\sum M_X, \sum M_Y, \sum M_Z$ represent the total moment components due to water and wind influence in the three axes; $\sum M_{X(M)}, \sum M_{Y(M)}, \sum M_{Z(M)}$ indicate the total mechanical moment components in the three axes; and J_X, J_Y, J_Z correspond to the moments of ship inertia in the body axis.

The ship path coordinates (x_g, y_g, z_g) at the center of gravity is calculated according to the following equations:

$$x_g = V_X \cdot \cos \varphi \cdot \cos \psi + V_Y (\sin \theta \cdot \cos \varphi \cdot \sin \psi - \cos \theta \cdot \sin \varphi) + \omega (\cos \theta \cdot \cos \varphi \cdot \sin \psi - \sin \theta \cdot \sin \varphi), \tag{11}$$

$$y_g = V_X \cdot \sin \varphi \cdot \cos \psi + V_Y (\sin \theta \cdot \sin \varphi \cdot \sin \psi - \cos \theta \cdot \cos \varphi) + \omega (\cos \theta \cdot \sin \varphi \cdot \sin \psi - \sin \theta \cdot \cos \varphi), \tag{12}$$

$$z_g = -V_X \cdot \sin \psi + V_Y \sin \theta \cdot \cos \psi + \omega \cdot \cos \theta \cdot \cos \psi. \tag{13}$$

The total components of forces and moments on the ship are defined by a set of equations consisting of several summands, which include the forces and moments on bare hull, the influence of steering devices (rudders and propellers), and the influence of external forces and moments (aerodynamic, current, wave, shallow waters, channel geometry). However, for the present paper, the simulations were carried out with the ship sailing in calm deep waters and with no rudder angle (amidships). With this premise, moving in calm deep water, the ship is affected by the hydrodynamic forces at the bare hull, the buoyancy forces, the stability forces, the inertia forces, and the forces on the ship's propellers and steering arrangement. Moreover, at the same time, the forces on the ship's propellers and steering gears depend on the ship control system parameters.

The hydrodynamic forces and moments on the ship are usually defined as the result of ship model experiment, and the measurements are usually performed in the body axes at given values of kinematics parameters, such as drift angle and rudder angle.

On one hand, rudders of different shapes are the most commonly used as a ship steering device. The hydrodynamic force on the rudder depends on the ship motion kinematic parameters, the rudder geometry, its relative area, the rudder angle, the propeller operating conditions, etc. The ship hull and propeller influence the hydrodynamic force on the rudder. Furthermore, the rudder and propeller affect the hydrodynamic characteristics of the bare hull. Therefore, the ship mathematical models consider the interaction forces and moments of ships equipped with different rudder configurations. On the other hand, in the mathematical models, when geometric parameters are considered, two propeller types were used: fixed pitch propeller (FPP) and controllable pitch propeller (CPP). For the models in which two propellers are included, each propeller thrust is calculated, and the total thrust and moment are calculated as the sum of the corresponding values.

2.3. Testing Simulations: Data Collection

During the simulations, different ship models were tested (bulk carrier, tanker, VLCC, passenger ferry, container carrier, and LNG), each having very different ship's particulars. Furthermore, in some of these models, different loading conditions were studied, resulting in a total of 12 studied cases, which can be considered representative enough of the most common ships in the merchant fleet. Table 1 includes the main ship's particulars affecting the maneuverability of the different used ship models.

Table 1. Ship's particulars of the used models.

No.	Type	D (t)	L (m)	B (m)	Stern Draft (m)	Bow Draft (m)	BC
1	Bulk carrier	23,565	182.9	22.6	7.6	7.6	0.76
2	Bulk carrier	23,565	182.9	22.6	10.7	10.1	0.77
3	Tanker	77,100	242.8	32.2	12.5	12.5	0.79
4	VLCC	63,430	261.3	48.3	9.0	5.8	0.68
5	VLCC	159,584	261.3	48.3	16.9	16.5	0.76
6	Pass ferry	11,046	145.0	25.2	5.3	5.1	0.62
7	Container	41,172	279.0	40.4	9.0	6.0	0.49
8	Container	93,130	279.0	40.4	14.0	14.0	0.59
9	LNG	149,332	315.2	50.0	12.5	12.5	0.76
10	LNG	111,061	315.2	50.0	9.6	9.6	0.73
11	LNG	130,196	315.2	50.0	10.5	10.5	0.79
12	LNG	143,136	315.2	50.0	12.3	11.7	0.76

To find the CLR position with the ships sailing ahead at any constant speed, the following premises were considered:

- All simulations that started with the ship from a stationary position (zero speed).
- The main engine(s) running at the five modes (RPM) of engine telegraph orders: stop (STP); dead slow ahead (DSA); slow ahead (SA); half ahead (HA); and full ahead (FA).
- The rudder was set at amidships and in follow-up mode.
- Calm conditions were selected, without the influence of waves and wind force.
- Navigation was performed in deep and open waters, without the influence of other ships, shallow waters, channels, or bank effects.
- After applying the transversal virtual force, the corresponding longitudinal position was set when no turning moment was observed ($ROT = 0$) once the ship reached a constant speed at the corresponding engine telegraph (RPM).
- Different types of ships and, in some cases, different loading conditions, cause differences in the maximum and constant speeds according to the same engine telegraph

order (RPM). For this reason, Table 2 includes the speeds achieved corresponding to the five different engine telegraph orders (RPM).

Table 2. Maximum speed attained according to the RPM of the different ships' and loading conditions.

No.	Type	STP	Speed (Knots)			
			DSA	SA	HA	FA
1	Bulk carrier	0.0	3.4	5.2	6.6	10.5
2	Bulk carrier	0.0	3.6	5.2	6.6	10.5
3	Tanker	0.0	5.5	8.2	11.1	13.3
4	VLCC	0.0	4.9	6.8	10.3	13.5
5	VLCC	0.0	4.0	5.6	9.3	11.5
6	Pass ferry	0.0	5.6	11.0	15.0	18.5
7	Container	0.0	6.3	15.9	22.4	26.5
8	Container	0.0	6.3	13.5	18.1	19.5
9	LNG	0.0	7.4	10.3	14.1	17.2
10	LNG	0.0	7.8	10.8	14.5	18.1
11	LNG	0.0	7.3	10.3	14.4	17.7
12	LNG	0.0	7.4	10.3	13.9	17.3

To locate the position of the CLR, i.e., the neutral point from a maneuverability point of view, a virtual force of 20.0 tonnes was applied transversally to the ship's centerline. It was necessary to carry out a large number of tests along the ship's length until a stable condition is noted, where the ROT was equal to zero. In Figure 2, the virtual force transversally applied from the starboard side of the LNG carrier can be observed from the instructor station, and in Figure 3, the full vision of this model during the navigation is represented.

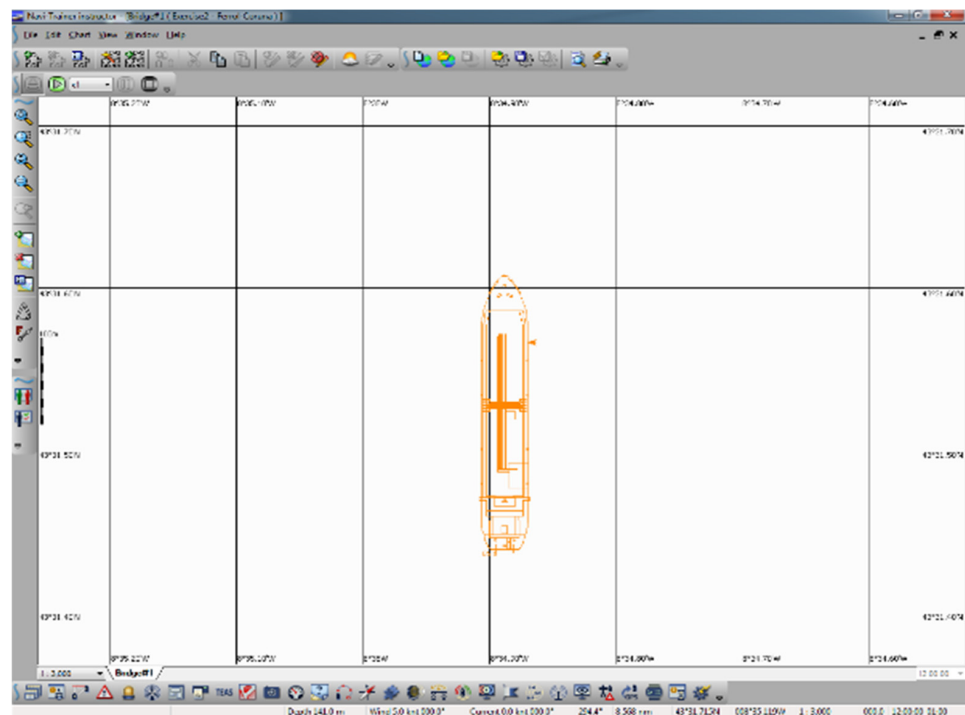


Figure 2. A 2D vision of Transas simulator from the instructor's station.



Figure 3. Bridge view of Transas simulator from the instructor’s station.

Although the conning display shows the value of instantaneous ROT (nil; + starboard side; – port side), in the simulator, there is a specific panel of ship speed indicators for the ship’s longitudinal and transverse speeds, both on the bow and on the stern. Therefore, despite noting a constant ROT = 0 in the stable condition, a detailed observation of the tendency of bow and stern speeds was carried out. Moreover, when the CLR position was located after applying the transversal virtual force to the centerline, the transverse speed of the bow and the stern had to be the same, and in the same direction.

In all simulations, the magnitude of the applied virtual force was 20.0 tonnes. Although the magnitude of this force could vary in different simulations, the only difference would be that the transverse speed of the bow and the stern would be different (higher or lower), but the CLR position would be the same. In the conning display in Figure 4, a forward speed of 7.08 knots for an ROT = 0 can be observed.



Figure 4. Conning display for a simulation with an LNG carrier.

Furthermore, the aim of applying the virtual force transversally to the ship’s centerline was to avoid creating a new forward/stern speed component.

3. Results

Identification of the More Relevant Variables

Different procedures were employed to identify the initial relation between variables, wherein the most important ones were One-Way ANOVA and random forest. This ANOVA study showed a clear relation between the distances of the application point of a virtual force that results in an ROT equal to zero. This distance is sampled from the stern and abbreviated as distance from stern (DS), and the numerical identification employing code (C) of different types of ships is inserted in Table 3.

Table 3. Code of types of ships.

Code	Type of Ship
1	Bulk carrier
2	Tanker
3	VLCC
4	Passenger ferry
5	Container ship
6	LNG carrier

This initial study showed a clear relation between the DS and the ship displacement (D), ship speed (S), bow draft (BD), length (L), beam (B), block coefficient (BC), and the ratio of length/beam (L/B) and beam/mean draft (B/MD). Table 4 presents the abbreviations corresponding to each variable and the corresponding significance.

Table 4. Significance of each variable.

Displacement	D	0.000
Speed	S	0.000
Bow Draft	BD	0.002
Stern Draft	SD	0.034
Trim	T	0.570
Mean Draft	MD	0.862
Length	L	0.000
Beam	B	0.000
Block Coefficient	BC	0.000
Length/Beam	L/B	0.000
Beam/Mean Draft	B/MD	0.059
Code	C	0.000

Some of the variables or relationships between, for instance, L/B and B/MD, are included in this study because, as it is known, they influence the course stability and can affect the CLR position, although it has been observed that this does not occur with great influence.

Based on these results, a multivariable curve fitting was conducted. In particular, a response surface based on the indicated variables showed a determination factor of the model test of 79.6% when employing all the indicated variables, as can be observed in Equation (14):

$$\begin{aligned}
 DS = & -2624 + 250 \cdot C - 0.00869 \cdot D + 35.5 \cdot S + 51.8 \cdot BD - 3.03 \cdot L + 37.4 \cdot B + 769 \cdot BC + \\
 & + 191 \cdot \left(\frac{L}{B}\right) - 18 \cdot \left(\frac{B}{MD}\right) - 28.1 \cdot C^2 - 0.6392 \cdot S^2 - 1.35 \cdot BD^2 + 0.061 \cdot C \cdot S + 0.000215 \cdot D \cdot S - \\
 & - 1.04 \cdot S \cdot BD + 0.144 \cdot S \cdot L - 1.588 \cdot S \cdot B + 0.9 \cdot S \cdot BC - 2.92 \cdot S \cdot \left(\frac{L}{B}\right) + 3.27 \cdot S \cdot \left(\frac{B}{MD}\right)
 \end{aligned}
 \tag{14}$$

Despite this, as it can be observed from Figure 5, it is not good enough to predict the DS with clear differences between the data obtained from the simulator and the one proposed by the mathematical model.

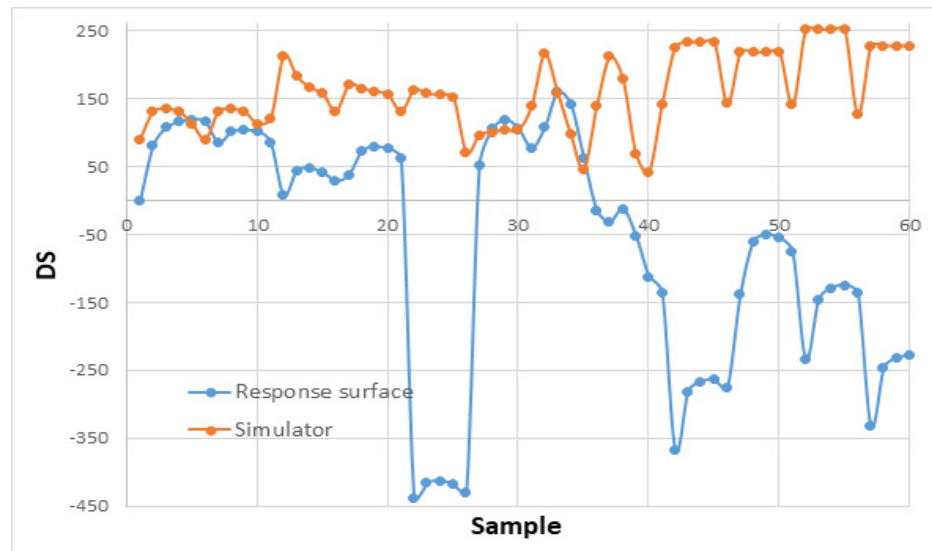


Figure 5. Comparison between simulator and response surface predictions.

This initial test was of interest but had excessive errors in its predictions, which could be associated with the use of redundant variables. As a consequence of this, a random forest machine learning algorithm allowed us to identify the importance of the selected variables, as can be observed from Figure 6.

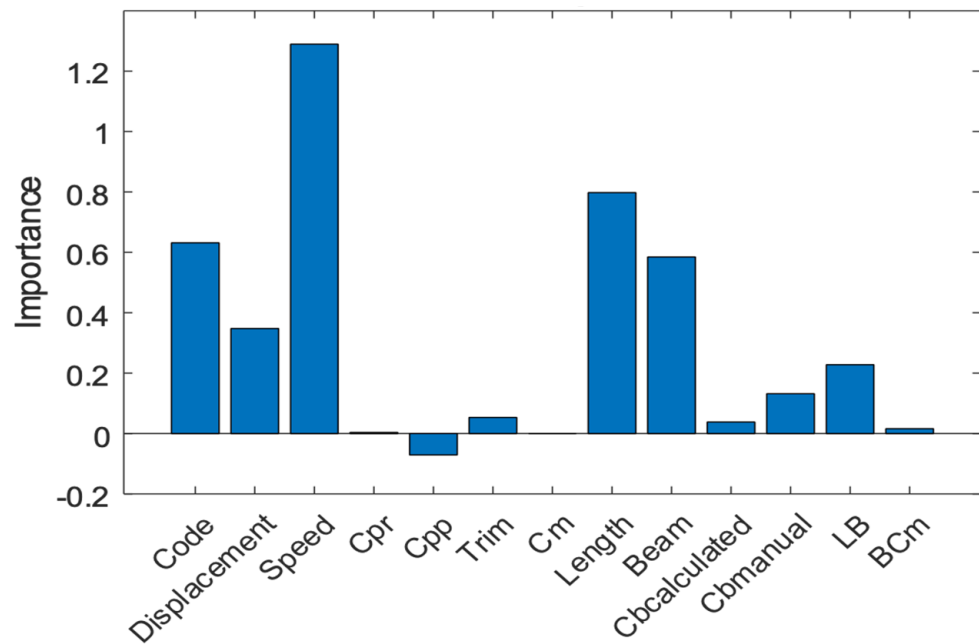


Figure 6. Random forest algorithm to predict the importance of each variable.

As can be deduced from Figure 6, the two most relevant variables highlighted by the random forest analysis are ship speed (the most relevant) followed by the ship length. Other variables are of lesser importance, such as the type of ship (code) and the beam of the ship.

Moreover, other variables showed nearly no importance like BD, SD, Trim, MD, BC, and B/MD. Due to this, several models were trained in accordance with the well-known artificial intelligence (AI) methodology and with all the selected variables employed in the response surface. In accordance with the determination factor and the MSE obtained, the 15 more-accurate models were ordered as can be observed from Table 5.

Table 5. More-accurate AI models (employing all the selected variables: ship speed, ship length, type of ship, beam of the ship).

	MODEL	RMSE	MSE	R ²	MAE
1	Gaussian Process Regression	18.446	340.26	0.88946	11.428
2	Gaussian Process Regression	19.49	379.85	0.8766	11.98
3	Gaussian Process Regression	21.72	471.75	0.84674	13.366
4	Gaussian Process Regression	22.264	495.69	0.83896	15.028
5	SVM	23.895	570.99	0.8145	13.659
6	SVM	27.499	756.18	0.75434	17.852
7	Tree	28.186	794.43	0.74191	21.624
8	Tree	28.186	794.43	0.74191	21.624
9	Ensemble	28.454	809.66	0.73696	20.54
10	SVM	28.65	820.83	0.73333	19.795
11	SVM	32.956	1086.1	0.64715	24.65
12	Ensemble	36.33	1319.9	0.57121	26.814
13	Stepwise Linear Regression	37.891	1435.8	0.53356	27.865
14	Linear Regression	39.578	1566.4	0.49112	28.67
15	SVM	40.338	1627.2	0.47137	28.608

From Table 5, it can be concluded that Gaussian models showed a higher determination factor when employing the previously selected variables. Nevertheless, due to the reduced determination factor, a simplification of the employed variables was performed in accordance with the random forest result, and the training process of the AI models was performed again. In this sense, by deleting the variable code (C) the average determination factor was 0.87 in a Gaussian model. When the block coefficient (BC) was deleted, the support vector machine (SVM) demonstrated a determination factor higher than before (0.92), as is shown in Figure 7. The relation of this SVM model between the sampled value (true) and the value predicted by the model (predicted) is shown in Figure 8.

Continuing with the simplification of variables, by deleting the bow draft (BD), a higher determination factor of 0.84 was obtained for neural network (NN) models (feedforward 10 layers). Finally, by deleting ship displacement (D), the Gaussian models obtained a determination factor of 0.93, and if the beam (B) was deleted (only the ship length (L) and ship speed (S) remain), the determination factor was 0.84 with neural networks, as can be seen in Table 6.

Based on these results, the validation of the selected model (NN) in predicting DS with respect to these two variables is presented through a graphical representation in Figure 9. In this Figure, the relationship between the DS obtained by the simulator and the one predicted by the NN model employing ship length (L) and speed (S) can be observed. It is clear that the elevated accuracy of the model is in this working range.

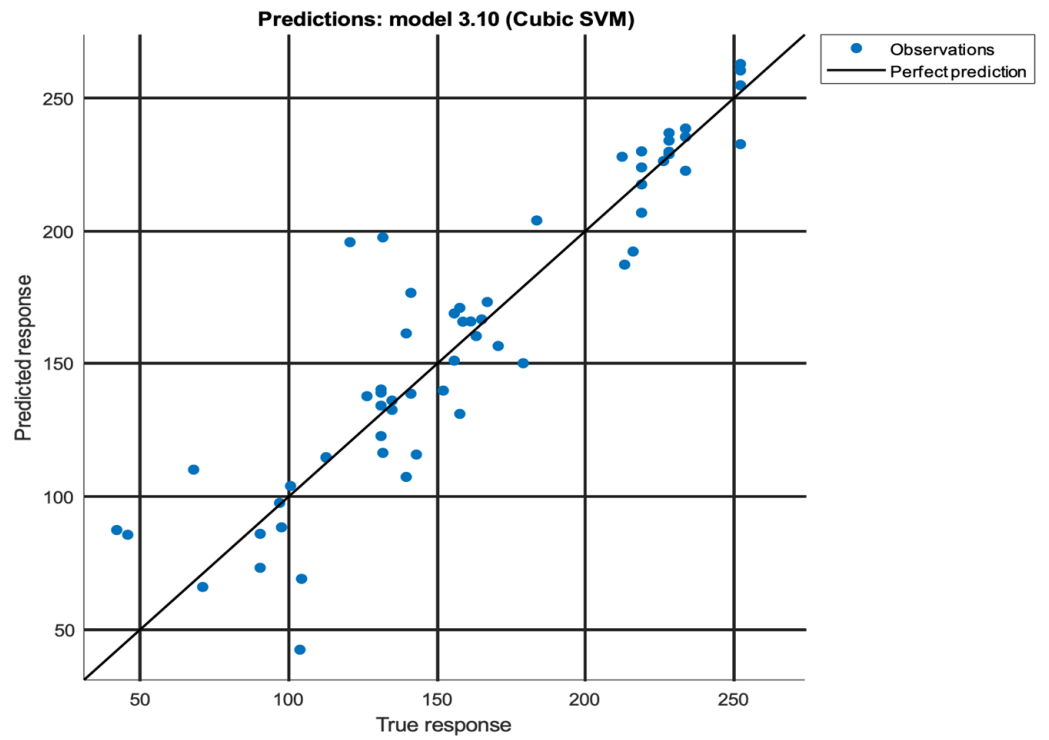


Figure 7. Comparison between observations and predictions by employing a SVM ($R^2 = 0.92$).

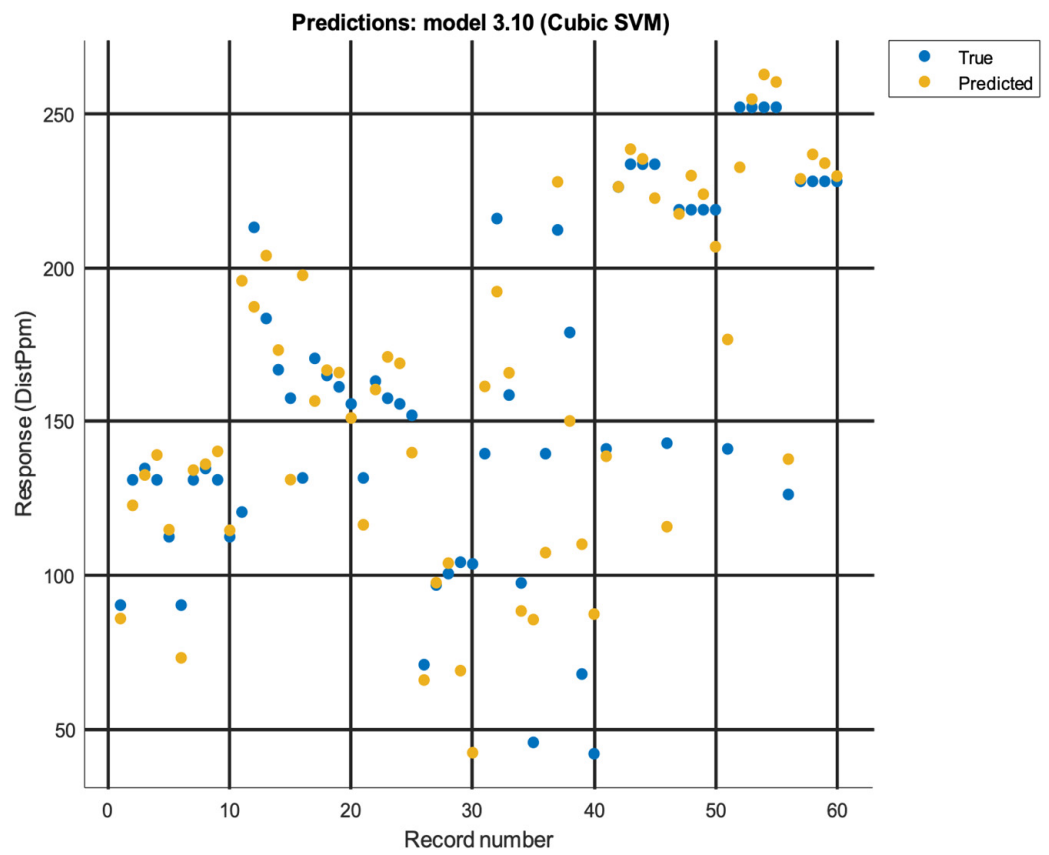


Figure 8. Comparison between the sampled value and the predicted (SVM model) ($R^2 = 0.92$).

Table 6. AI models that predict DS with two predictors (speed and length).

	MODEL	RMSE	MSE	R ²	MAE
1	Neural Network	22.004	484.19	0.84616	14.663
2	SVM	22.548	508.41	0.83847	15.205
3	SVM	24.419	596.3	0.81054	16.037
4	Gaussian Process Regression	24.43	596.83	0.81037	13.97
5	Neural Network	27.053	731.85	0.76747	19.493
6	Gaussian Process Regression	27.727	768.81	0.75573	16.338
7	Kernel	28.052	786.93	0.74997	19.48
8	Neural Network	28.223	796.54	0.74692	18.318
9	Gaussian Process Regression	28.444	809.06	0.74294	16.409
10	Ensemble	28.559	815.59	0.74087	20.107
11	SVM	29.216	853.58	0.7288	19.655
12	Neural Network	29.397	864.2	0.72542	19.25
13	SVM	29.605	876.47	0.72152	18.863
14	Gaussian Process Regression	29.78	886.83	0.71823	18.242
15	Tree	32.695	1069	0.66036	23.559

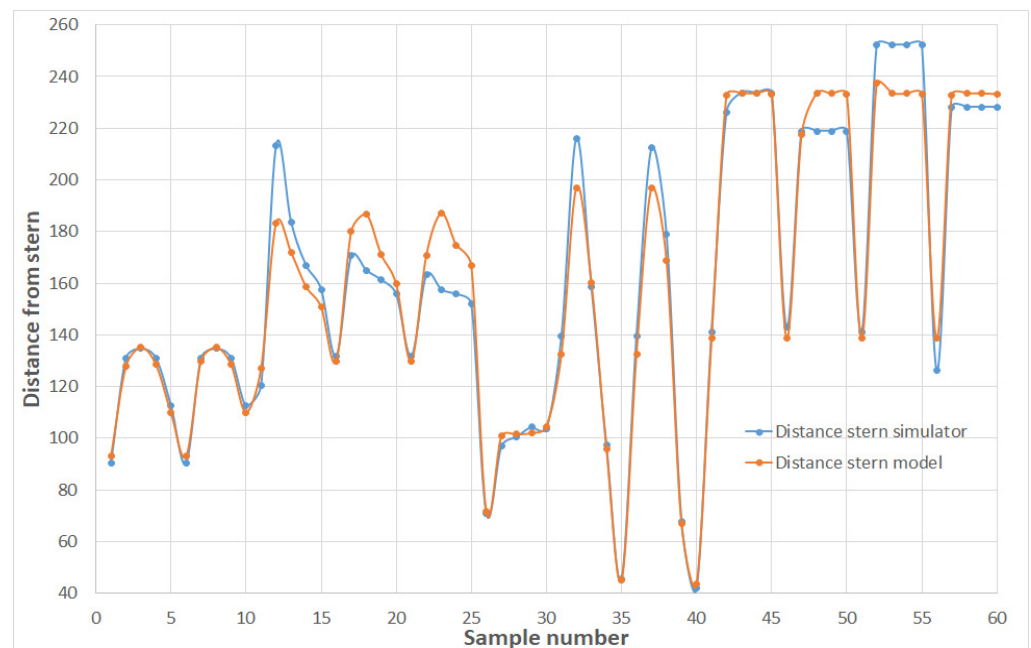


Figure 9. Comparison of the DS obtained from the simulator and the NN model.

In accordance with the interesting accuracy of the obtained NN model, a combination of the input variables (ship speed and length) was employed to identify the map of the process, as shown in Figure 10.

This 3D chart shows the evolution of the distance from the stern (DS) where the force is applied until an ROT = 0 is reached, or, an equivalent outcome of a pure lateral displacement of the ship is obtained. As can be observed from Figure 10, the distance reached is nearly 200 m from the stern when the ship length is about 320 m and the ship speed is null (0 knots). When the ship speed increases, for the same ship length, the distance is reduced till it reaches 0 m (stern) at 25 knots (blue region).

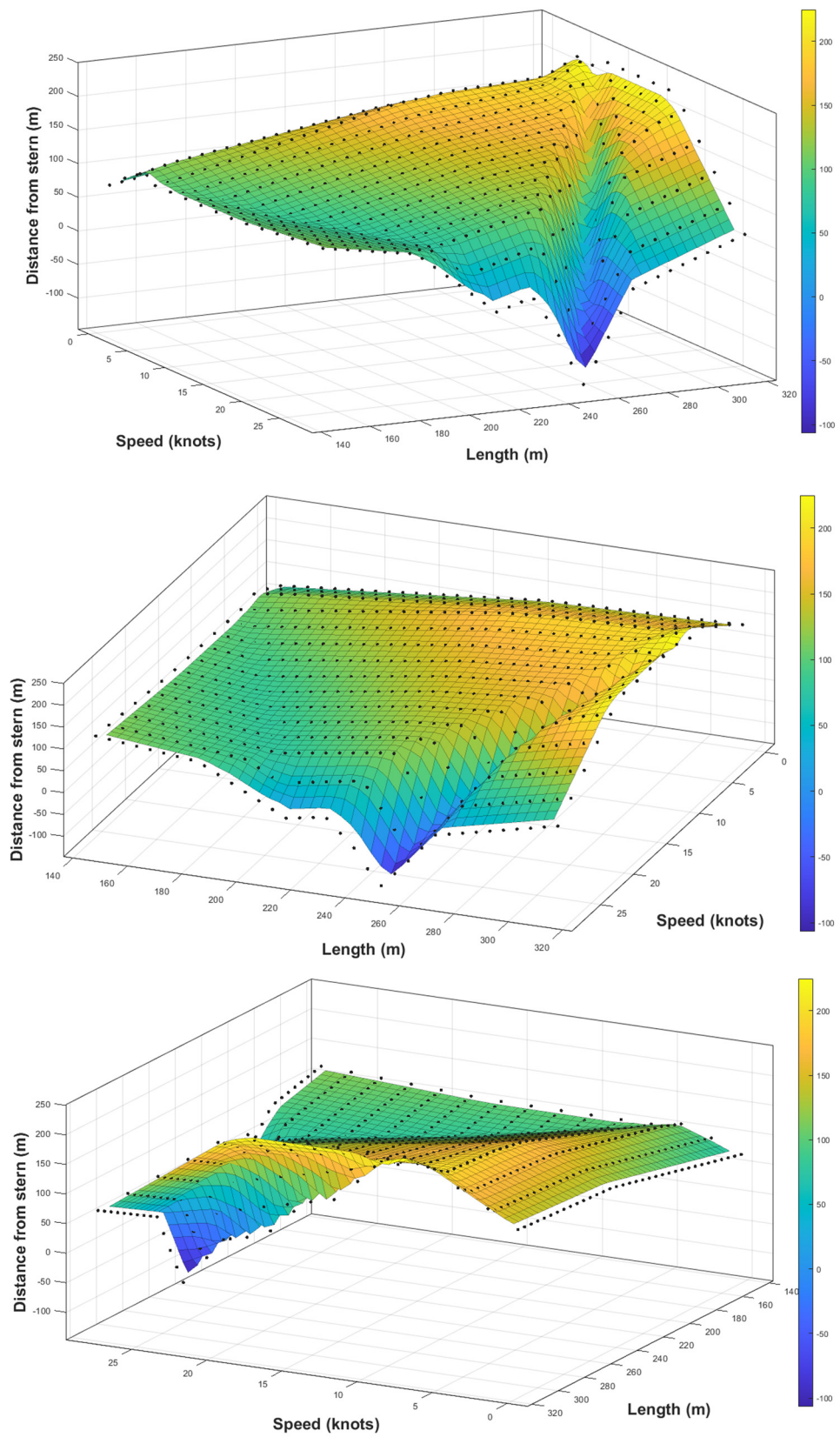


Figure 10. Prediction of the DS versus ship speed and ship length.

Despite this, there is a drop in the middle of the surface that implies the point of application of the force experienced a fast reduction in the distance to the stern, or a sudden fast reduction in the distance when the speed increases and the ship length is over 240 m.

In ships with a length of less than 240 m, this sudden reduction in the distance to the stern does not exist.

It is of interest to obtain an idea about the relations between DS and ship speed. Consequently, a representation of this evolution for the same ship length is shown in Figure 11.

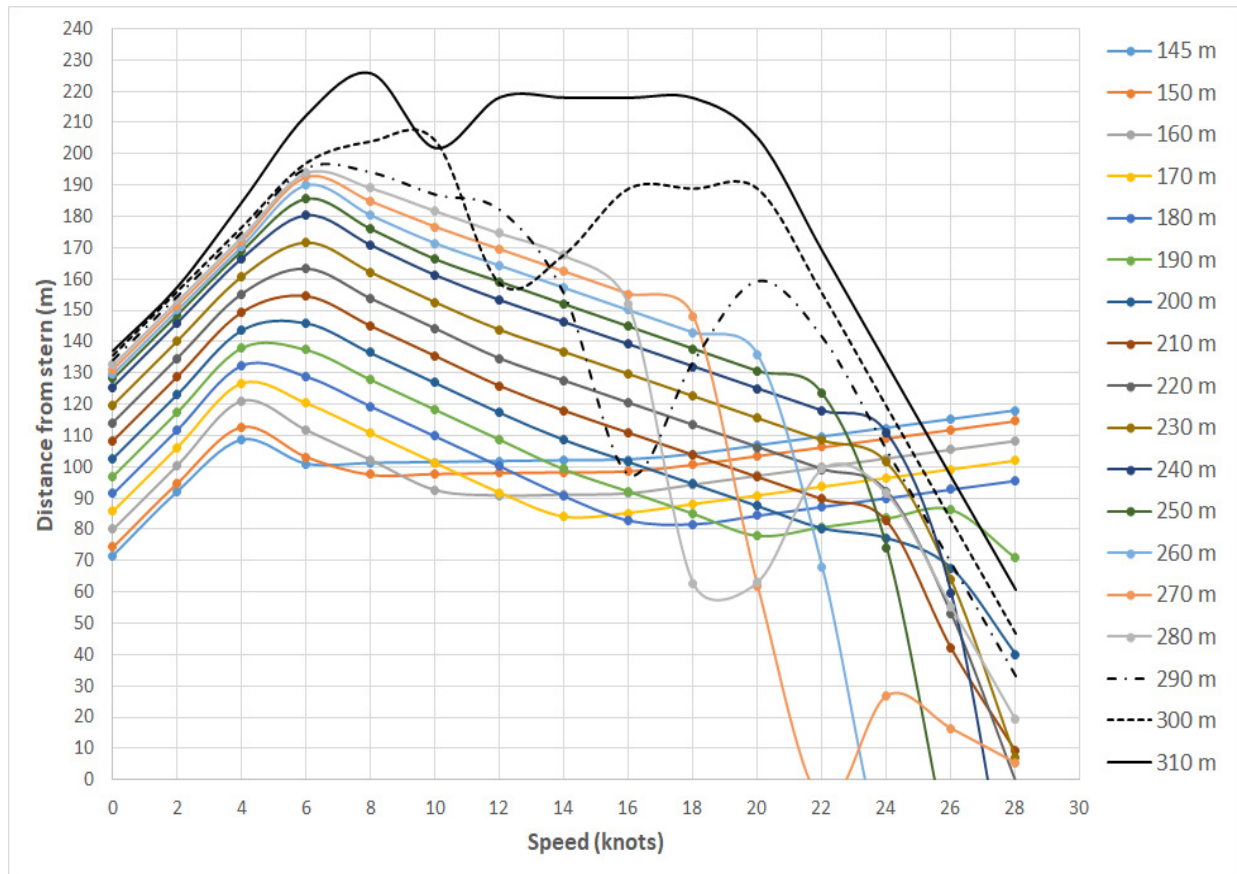


Figure 11. Evolution of DS at different ship speeds for each ship length.

From Figure 11, it can be concluded that there is a proportional increase in DS with the ship speed from 0 to 6 knots. From this point, there is a linear decrement of the DS with respect to the ship speed in a range from roughly 4 to 20 knots. There are extreme ship lengths (from 290 m to 310 m) at which there is no linear decrement, and a certain nonlinear evolution is observed in Figure 11.

To determine a practical and useful relation for this effect, the initial DS must be analyzed at zero knots, as shown in Table 7.

From Table 7 and Figure 12, a linear relation between DS at 0 knots and ship length in accordance with Equation (14) can be observed:

$$DS_0 = 0.4195 \cdot L + 16.577 \tag{15}$$

Equation (15) tells us the initial DS for any ship length (L). At the same time, it is possible to obtain a model of the initial linear relation until it reaches 6 knots based on the curve fitting of Figure 13 for a ship length of 200 m and generalized by Equation (16) with a determination factor of 0.91. Equation (16) is a linear relation with a constant value defined by the DS at 0 knots obtained by Equation (15):

$$DS = 7.5201 \cdot S + DS_0 \tag{16}$$

Table 7. DS at 0 knots for different ship lengths.

	Ship Length	DS at 0 Knots
1	145	71.48
2	150	74.32
3	160	80.01
4	170	85.69
5	180	91.37
6	190	97.06
7	200	102.74
8	210	108.42
9	220	114.10
10	230	119.79
11	240	125.47
12	250	128.15
13	260	129.64
14	270	131.14
15	280	132.64
16	290	134.13
17	300	135.63
18	310	137.70

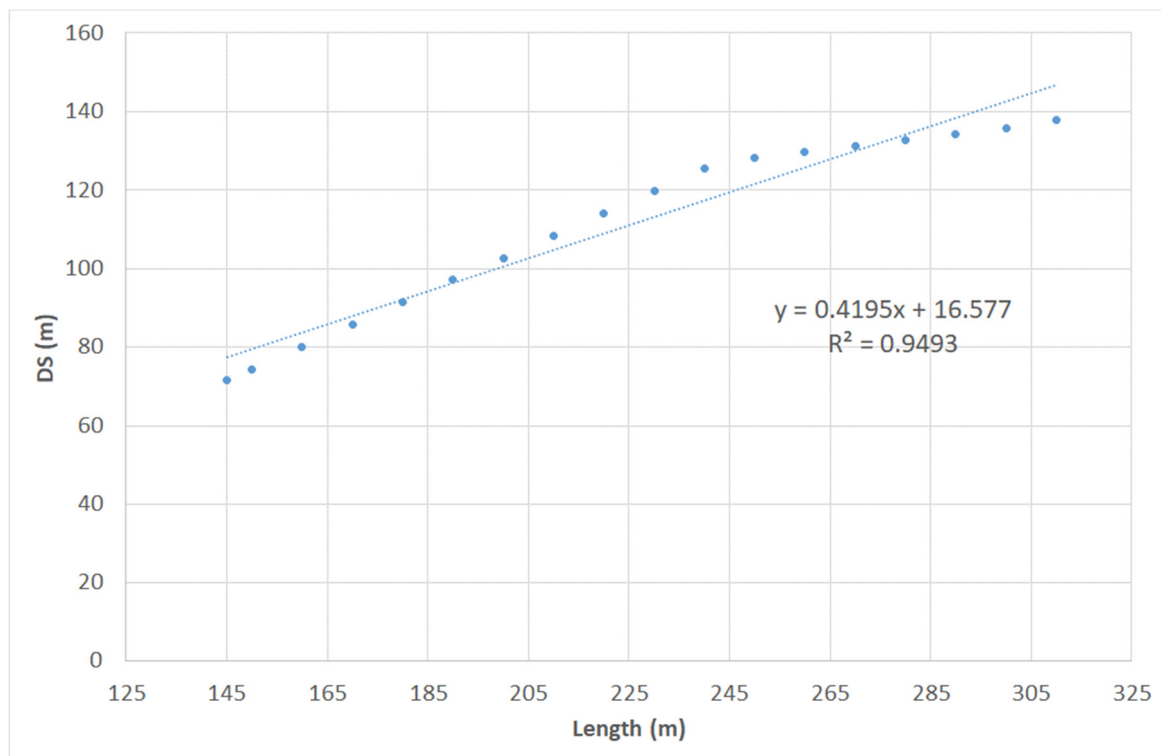


Figure 12. DS at 0 knots for different ship lengths.

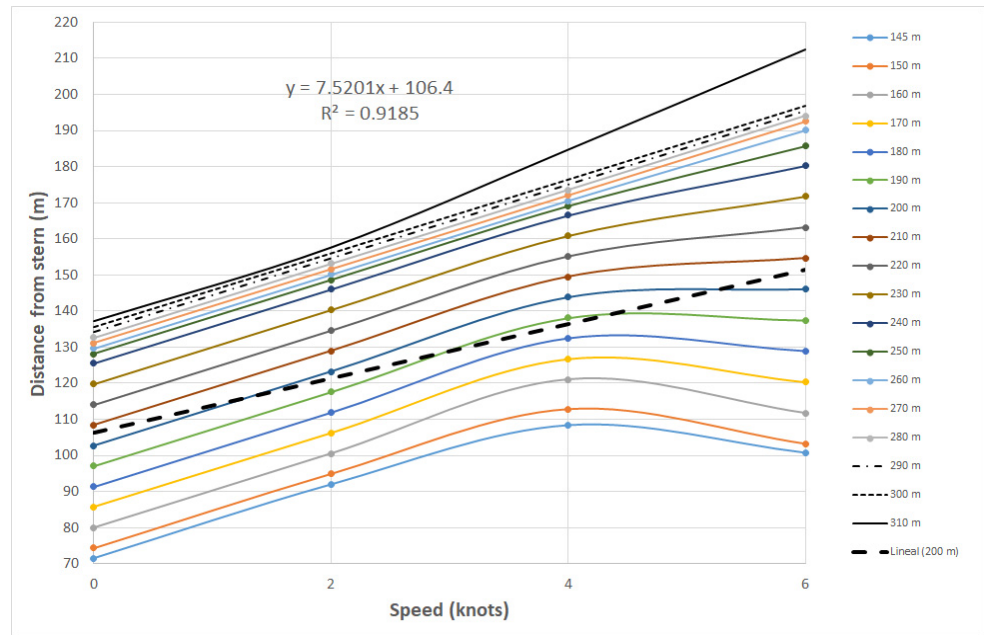


Figure 13. Linear relation between DS and sheep speed (range 0 to 6 knots).

DS0 is the DS at 0 knots defined by Equation (15). A more useful Equation (17) is obtained when Equation (15) is included in Equation (16):

$$DS = 7.5201 \cdot S + 0.4195 \cdot L + 16.577. \tag{17}$$

This new equation is of great interest for different maneuvering situations on-board. By applying the same methodology, a new mathematical model can be obtained for ship speeds higher than 6 knots, as can be observed in Figure 14 and represented in Equation (18) for a ship of 210 m length with a determination factor of 0.99.

$$DS = -4.1163 \cdot S + 177.35 \tag{18}$$

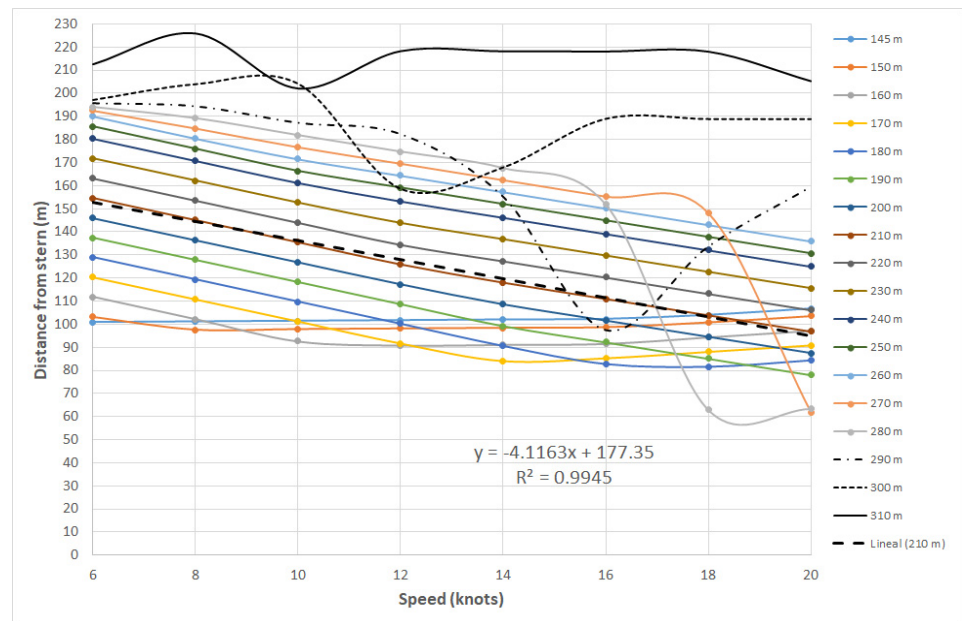


Figure 14. Linear relation between DS and ship speed (range 6 to 20 knots).

In conclusion, two equations were obtained that define the relation of DS with ship length for two ship speeds; from 0 to 6 knots and from 6 knots to 20 knots. These two new equations are of special interest for shiphandlers with tugboat operations in port maneuvering. Finally, it must be highlighted for speeds higher than 20 knots that there are nonlinear tendencies that make the linear model inaccurate.

4. Discussion

As previously discussed, and according to the literature, the only understanding of the tradition PP is not exact for the maneuvering purposes of shiphandlers. Moreover, in many circumstances, knowing the CLR position is more important than the PP position from a navigation's safety and efficiency point of view. The review literature shows that specific studies about the CLR position are limited, indicating its approximate position at the port operation speeds, or when the ship has trimmed by forward or aft. Moreover, it is assumed that CLR movement is rarely more than 10% of the ship's length in the direction of the ship's motion. As these research works are not too specific because, for instance, the ship's particulars and loading conditions are included, in this paper, a new approach for calculating the CLR positions were addressed. For this mission, a full bridge simulator and IA techniques were employed to obtain novel mathematical models and new 3D charts which can be easily applied by the shiphandlers. These results allow us to carry out safer and more efficient maneuverings in restricted waters, solving the problems raised by the presence of larger ships in the same restricted areas.

In addition to the PP, the knowledge of the CLR position is essential for the shiphandler to ensure the safety of navigation, to optimize the number of tugboats required, and even to avoid accidents. An example of this was the collision of the *m/v Dali* against the Francis Scott Key Bridge in Baltimore on March 2024, resulting in several deaths and million-dollar losses. In this case, if a tugboat had been available alongside the assisted vessel, the knowledge of the exact location of the CLR, where it can push/pull to generate only sideway motion, could have prevented the collision, considering that the problems on board were noted well in advance and the speed was not too high. If this force was not applied at CLR by escorting the assisted vessel by the stern, for example, the turning momentum could have caused the ship's stern to collide with the bridge as well.

During the multiple simulations carried out, before noting the exact position of the virtual force needed to reach an $ROT = 0$, as the speed increased, oscillations in the ROT values of both sides (port and starboard sides) were recorded due to the influence, for instance, of the propeller's rotation in the first moments. Nevertheless, in the case of the passenger ferry or LNG carriers, equipped with tandem propellers, this effect was not recorded due to the compensation that occurs between the two propellers rotating in opposite directions.

5. Conclusions

In the present paper, the CLR position of different types of ships and in different loading conditions was studied. Data collection was obtained after carrying out a high number of simulations in a full mission bridge simulator which, once the used models were certified and shown, was accepted by international organizations as valid for training and obtaining relevant conclusions.

The most common variables affecting the ship's behavior from a maneuvering point of view (PP and CLR) were analyzed, and after using neural networks, 15 novel models of the CLR position from the stern were obtained. However, it was necessary to simplify some variables to obtain an acceptable determination factor for neural network models, which was achieved with a combination of ship length and speed. Finally, very simple and novel equations relating these two variables were obtained, which can be used very easily by any shiphandler on board.

Future studies could be conducted to validate these results in towing tanks or in full-scale trials on board any type of ship. Moreover, it would be interesting to relate the presented models of CLR position with the position of the pivot point.

Furthermore, it would be interesting if in the conning display (both in bridge simulators and on the real bridge on board), not only the instantaneous values of the ROT, but also the position of the pivot point are shown. Therefore, future investigations could be guided to calculate the instantaneous value of the peripatetic pivot point along the ship’s length. Knowing both data, the prediction of the ship’s behavior during the shiphandling would result in a more efficient and safer maneuver.

Finally, future studies can be focused on presenting the results of the novel mathematical models obtained in the conning display of the used bridge simulator in order to obtain the reaction during the maneuvering purposes of the users. In this way, it would be empirically tested whether CLR position prediction can improve maneuvering efficiency with the assistance of tugboats.

Author Contributions: Conceptualization, J.M.P.-C., F.J.L.-C. and J.A.O.; methodology, J.M.P.-C., F.J.L.-C., A.S.-D., E.A.P., G.C.-F. and J.A.O.; software, J.M.P.-C., F.J.L.-C. and J.A.O.; validation, J.M.P.-C., F.J.L.-C., A.S.-D., E.A.P., G.C.-F. and J.A.O.; formal analysis, J.M.P.-C., F.J.L.-C., A.S.-D., E.A.P., G.C.-F. and J.A.O.; investigation, J.M.P.-C., F.J.L.-C. and J.A.O.; resources, J.M.P.-C., F.J.L.-C., A.S.-D., E.A.P., G.C.-F. and J.A.O.; data curation, J.M.P.-C., F.J.L.-C., A.S.-D., E.A.P., G.C.-F. and J.A.O.; writing—original draft preparation, J.M.P.-C., F.J.L.-C. and J.A.O.; writing—review and editing, J.M.P.-C., F.J.L.-C., A.S.-D., E.A.P., G.C.-F. and J.A.O.; visualization, J.M.P.-C., F.J.L.-C., A.S.-D., E.A.P., G.C.-F. and J.A.O.; supervision, J.M.P.-C. and J.A.O. All authors have read and agreed to the published version of the manuscript.

Funding: This research received no external funding.

Institutional Review Board Statement: Not applicable.

Informed Consent Statement: Not applicable.

Data Availability Statement: Data are contained within the article.

Conflicts of Interest: The authors declare no conflicts of interest.

Appendix A

Table A1. Symbols and their definitions.

Symbol	Definition
$\Sigma F_X, \Sigma F_Y, \Sigma F_Z$	Total force components due to water and wind influence in the three axes
$\Sigma F_{X(M)}, \Sigma F_{Y(M)}, \Sigma F_{Z(M)}$	Total mechanical force in the three axes
B	Ship’s beam
BC	Block coefficient
BD	Bow draft
C	Code
CLR	Center of lateral resistance
CPP	Controllable pitch propeller
D	Ship’s displacement
DS	Distance from stern
DS ₀	Distance from stern at 0 knots
Dr	Ship’s draught
DSA	Dead slow ahead
FA	Full ahead
FPP	Fixed pitch propeller
HA	Half ahead
L	Ship’s length
LNG	Liquefied natural gas carrier
m	Meters
m _A	Ship’s mass

Table A1. Cont.

Symbol	Definition
MD	Mean draft
NN	Neural networks
PP	Pivot point
ROT	Rate of turn
RPM	Revolutions per minute
S	Speed
SA	Slow ahead
SD	Stern draft
STCW	International Convention on Standards of Training, Certification, and Watchkeeping for Seafarers
STP	Stop
SVM	Support vector machine
t	Tonnes
T	Trim
VLCC	Very large crude carrier
V_X, V_Y, V_Z	Ship velocity components in body axis
x_g, y_g, z_g	The ship path coordinates at center of gravity
IMO	International Maritime Organization
φ	Course angle
$\lambda_{11}, \lambda_{22}, \dots, \lambda_{66}$	Added masses
θ	Roll angle
ρ	Water density
$\omega_X, \omega_Y, \omega_Z$	Ship angular velocity components in body axis
ψ	Pitch angle

References

- Juszkiewicz, W.; Żukowska, A. The Use of the K-Sim Polaris Simulator in the Process of Automatic Assessment of Navigator Competence in the Aspect of Anticollision Activities. *Appl. Sci.* **2023**, *13*, 915. [\[CrossRef\]](#)
- Sellberg, C. Simulators in bridge operations training and assessment: A systematic review and qualitative synthesis. *J. Marit. Aff.* **2017**, *16*, 247–263. [\[CrossRef\]](#)
- Bradsaeter, A.; Madsen, A. A simulator-based approach for testing and assessing human supervised autonomous ship navigation. *J. Mar. Sci. Technol.* **2024**, *29*, 432–445. [\[CrossRef\]](#)
- Emre Seno, Y.; Seyhan, A. A novel machine-learning based prediction model for ship manoeuvring emissions by using bridge simulator. *Ocean Eng.* **2024**, *291*, 116411. [\[CrossRef\]](#)
- Gralak, R.; Muczyński, B.; Przywarty, M. Improving Ship Maneuvering Safety with Augmented Virtuality Navigation Information Displays. *Appl. Sci.* **2021**, *11*, 7663. [\[CrossRef\]](#)
- Sencila, V.; Zazeckis, R.; Jankauskas, A. The use of a full mission bridge simulator ensuring navigational safety during the Klaipeda seaport development. *TransNav Int. J. Mar. Navig. Saf. Sea Transp.* **2020**, *14*, 417–424. [\[CrossRef\]](#)
- Pérez-Canosa, J.M.; Orosa, J.A.; Pacheco, E.A. A New Understanding and Modelling of TSP and BP Indices Compared to Safety IMO Ship Requirements. *Appl. Sci.* **2021**, *11*, 7142. [\[CrossRef\]](#)
- Shang, H.; Zhan, C.; Liu, Z. Numerical Simulation of Ship Maneuvers through Self-Propulsion. *J. Mar. Sci. Eng.* **2021**, *9*, 1017. [\[CrossRef\]](#)
- Toma, A.; Oncica, V.; Atodiresei, D. The study of ships behavior during port maneuvering with tugs. *Mircea Batran Nav. Acad. Sci. Bull.* **2016**, *19*, 109–115. [\[CrossRef\]](#)
- Cauvier, H. The pivot point. In *The Pilot*; United Kingdom Maritime Pilot's Association: Cowes, UK, 2008; p. 295.
- Zinchenko, S.; Tovstokoryi, O.; Nosov, P.; Popovych, I.; Kyrychenko, K. Pivot point position determination and its use for manoeuvring a vessel. *Ships Offshore Struct.* **2022**, *18*, 358–365. [\[CrossRef\]](#)
- Pérez-Canosa, J.M.; Orosa, J.A. Proposal of a New Control System Making Use of AI Tools to Predict a Ship's Behaviour When Approaching the Synchronism Phenomenon. *Appl. Sci.* **2024**, *14*, 4517. [\[CrossRef\]](#)

Disclaimer/Publisher's Note: The statements, opinions and data contained in all publications are solely those of the individual author(s) and contributor(s) and not of MDPI and/or the editor(s). MDPI and/or the editor(s) disclaim responsibility for any injury to people or property resulting from any ideas, methods, instructions or products referred to in the content.